# Precise shape engineering of epitaxial quantum dots by growth kinetics

Sergio Bietti,[1] Juanita Bocquel,[2] Silvia Adorno,[1] Takaaki Mano,[3] Joris G. Keizer,[2]
Paul M. Koenraad,[2] and Stefano Sanguinetti[1,*]
[1]*LNESS and Dipartimento di Scienza dei Materiali, Universitá degli Studi di Milano Bicocca, Milano, Italy*
[2]*Department of Applied Physics, Eindhoven University of Technology, The Netherlands*
[3]*National Institute for Materials Science, Tsukuba, Japan*
(Received 15 May 2015; revised manuscript received 25 July 2015; published 19 August 2015)

We show that independent size and morphology engineering of epitaxial quantum dots can be obtained using a kinetically controlled quantum dot fabrication procedure, namely droplet epitaxy. Due to the far-from-equilibrium droplet epitaxy procedure, which is based on the crystallization, under As flux, of a nanometric droplet of Ga, independent and precise tuning of quantum dot size, aspect ratio, and faceting can be achieved. The dependence of the dot morphology on the growth conditions is interpreted and described quantitatively through a model that takes into account the crystallization kinetics of the Ga stored in the droplet under As flux.

DOI: 10.1103/PhysRevB.92.075425 PACS number(s): 81.15.Hi, 81.16.Dn, 68.65.Hb, 68.55.ag

## I. INTRODUCTION

Three-dimensional semiconductor epitaxial nanoislands, or quantum dots (QDs), exhibit a discrete spectrum of energy levels that make them the artificial equivalent of natural atoms [1]. Unlike and beyond natural atoms, QDs permits the fine tuning of their electronic properties by a precise engineering of their morphology. Both their single-particle and many-particle characteristics depend in a nontrivial way on the QD size and shape [2,3]. This reflects not only simple quantum-confinement physics, but also electronic-structure effects such as interband, intervalley, spin-orbit, and strain-induced state coupling [4,5], as well as electron–phonon scattering probability [6–8]. The QD shape allows for the engineering of the QD electronic states in order to effectively extend the performance of various optoelectronic devices [9], ranging from room-temperature QD-based intersubband detectors [10] and lasers [11] to semiconductor optical amplifiers [12], polarization-controlled single-photon emitters for quantum communication systems [13,14], and QD-based photovoltaic cells [15–17]. In particular, by controlling QD size and aspect ratio (the ratio between QD height and diameter), it would be possible to tune independently QD emission energy and electron-phonon interaction, two relevant properties in QD-based lasers, solar cells, and detectors.

One of the most common methods for QD fabrication is molecular beam epitaxy (MBE) of lattice-mismatched III-V semiconductor materials via the Stranski-Krastanov (SK) mode [18]. The SK mode exploits the self-assembly of pyramidal QDs driven by the relaxation of strain accumulated in the epilayer. Despite the high success of this technique, which led to a fundamental physical understanding of epitaxial QDs and to a large variety of applications [18–20], the available degree of freedom remains limited [21] due to energetic driven evolution of the SK-QD shape [22]. A possible pathway to circumvent the limitations of SK-QD self-assembly is the use of a different paradigm for the fabrication of QDs. In this respect, the exploitation of kinetics-controlled epitaxial nanoisland growth would overcome the limits imposed by the SK method, which is characterized by nanoisland shapes bound by an equilibrium set of facets that includes only stable surfaces [22].

Here we show that by using a kinetically driven epitaxial QD fabrication method, namely droplet epitaxy (DE) [23–26], a high degree of control over QD size, aspect ratio, and facet orientation angle (the angle between the substrate and the QD facet) is possible. GaAs/$Al_{0.3}GaAs_{0.7}$ DE-QDs, with volumes ranging from $10^2$ to $10^5$ nm$^3$, were obtained with a controlled aspect ratio ranging from 0.05 to 0.6 and a facet orientation angle from $10^\circ$ to $55^\circ$. This was achieved by an accurate drive of the crystallization kinetics via growth parameter control. The morphology of the GaAs/AlGaAs DE-QDs was investigated by means of atomic force microscopy (AFM) and cross-sectional scanning tunneling microscopy (X-STM). We propose a model to interpret and quantitatively describe the mechanism governing the relationship between QD shape and growth parameters based on Ga diffusion dynamics and crystallization during the exposure of the Ga liquid droplet to the As flux.

DE is an alternative growth procedure, based on MBE, for the self-assembly of epitaxial III-V semiconductor nanostructures. It relies on growth kinetics to form three-dimensional nanostructures. The DE procedure is based on the subsequent deposition of III and V column elements at specific temperatures and fluxes. In short, DE growth of nanostructures in an MBE environment proceeds as follows. A III-column element molecular beam is initially supplied for the formation of droplets on the substrate surface in vacuum, and subsequently an As flux is used for the crystallization of droplets into the III-As nanostructures. With a suitable selection of growth conditions, and by carefully controlling the group-III crystallization kinetics into a III-V semiconductor, it is possible to engineer the final shape of the nanocrystals from islands [25,27–29], rings [30,31], wires [32,33], and even more complex structures [34–39].

## II. EXPERIMENT

DE-QDs were grown in a conventional MBE apparatus on GaAs (001) substrates. After the growth of a 100 nm $Al_{0.3}Ga_{0.7}As$ buffer layer, we performed DE, which consists of the following:

*stefano.sanguinetti@unimib.it

 ©2015 American Physical Society

TABLE I. Growth parameters of the different sets of samples. Set $P$: variation in As BEP. Set $T$: variation in crystallization temperature. Set $V$: variation in Ga droplet volume. Set $V_{cap}$: variation in Ga droplet volume and capping procedure.

| Set | $P$ | $T$ | $V$ | $V_{cap}$ |
|---|---|---|---|---|
| Ga supplied (ML) | 2.5 | 2.5 | $V1 = 3$<br>$V2 = 2$<br>$V3 = 2.5$ | $C1 = 1.5$<br>$C2 = 2$<br>$C3 = 3$<br>$C4 = 5$ |
| Ga deposition $T$ (°C) | 350 | 350 | $V1 = 350$<br>$V2 = 350$<br>$V3 = 220$ | 200 |
| As BEP ($10^{-6}$ Torr) | $P1 = 50$<br>$P2 = 25$<br>$P3 = 10$<br>$P4 = 7.5$<br>$P5 = 5$ | 10 | 10 | 250 |
| Crystallization $T$ (°C) | 200 | $T1 = 150$<br>$T2 = 175$<br>$T3 = 200$<br>$T4 = 225$<br>$T5 = 250$ | 200 | 200 |
| Crystallization time (s) | 180 | 180 | 180 | 10 |
| QD density (cm$^{-2}$) | $6\times10^8$ | $6\times10^8$ | $6\times10^8$ to $1\times10^{10}$ | $2\times10^{10}$ |
| Ga droplet volume (nm$^3$) | $2.5\times10^4$ | $2.5\times10^4$ | $V1 = 3.7\times10^4$<br>$V2 = 1.8\times10^4$<br>$V3 = 1.8\times10^3$ | $C1 = 3\times10^2$<br>$C2 = 6\times10^2$<br>$C3 = 1.2\times10^3$<br>$C4 = 2.4\times10^3$ |

(i) Ga droplet formation by a supply of Ga without As flux (background As pressure was below $1\times10^{-9}$ Torr).

(ii) Crystallization of the Ga droplets into GaAs by a supply of $As_4$ flux with controlled pressures at various temperatures.

Droplet density and size are controlled during the Ga deposition step by the substrate temperature, the Ga flux, and the total amount of Ga deposited. The As pressure and substrate temperature during crystallization are used to control nanostructure morphology [30,35,37,40]. Three sets of samples ($P$, $T$, and $V$) were grown in this study. The detailed growth parameters are summarized in Table I. For sets $P$ and $T$, we prepared identical Ga droplets formed by a supply of 2.5 ML Ga at 350 °C. In set $P$, droplets were crystallized at 200 °C by a supply of different As beam equivalent pressure (BEP) ranging from $2.5\times10^{-5}$ to $5\times10^{-6}$ Torr. In set $T$, the As BEP was fixed at $1\times10^{-5}$ Torr while the droplets were crystallized at different substrate temperatures ranging from 150 to 250 °C. In set $V$, droplets of various size were crystallized under the identical conditions [supply of As (BEP $1\times10^{-5}$ Torr) at 200 °C]. The droplet size was varied by controlling the total amount of deposited Ga (from 2 to 2.5 ML) and the substrate temperature during deposition (from 250 to 350 °C). The latter parameter, by acting on droplet density (from $1\times10^{10}$ to $6\times10^8$ cm$^{-2}$) changes the amount of Ga stored in each single droplet. Within set $V$, we also grew a series of QDs with capping layer ($V_{cap}$) following the standard procedure for obtaining highly luminescent QDs, i.e., an uncapped annealing at 400 °C and a post-growth rapid thermal annealing at 750 °C [41]. In this subset, the Ga droplets were formed by a supply of 1.5–5 ML of Ga at 200 °C and subsequently crystallized at 200 °C by a supply of As flux of $2.5\times10^{-4}$ Torr. This subset is of special importance as it allows us to investigate the QDs after capping in their functional state. We expect that complete crystallization of the Ga droplets into GaAs QDs occurs along with a wetting layer with a thickness less than a bilayer, which originates from the change in surface reconstruction during the initial stages of Ga deposition [27,42].

All samples were characterized by AFM in tapping mode using ultrasharp tips with a 2 nm radius. In parallel, sample $V_{cap}$ was investigated by X-STM performed at 77 K under UHV conditions ($5\times10^{-11}$ Torr). The STM was operated in constant current mode on clean and atomically flat (110) and $(1\bar{1}0)$ GaAs surfaces obtained by *in situ* cleavage. This scanning probe technique allows us to investigate at the atomic scale the morphology of the DE-QDs after capping.

## III. RESULTS

For all sets of samples, a $c(4\times4)$ reconstruction was clearly visible in reflection high-energy electron diffraction (RHEED) patterns before Ga deposition. The single ML of Ga that required the subsequent onset of droplet formation as well as our experimental conditions [43] indicate that the $c(4\times4)\alpha$ phase is the most probable reconstruction at that initial stage. In all sets, after 1 ML of Ga was incorporated on

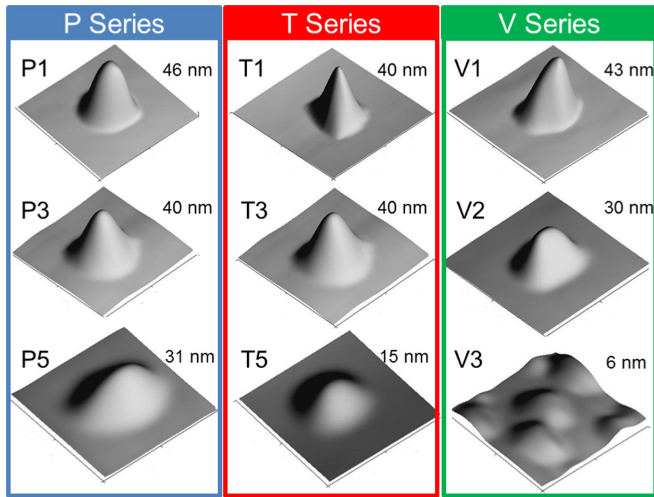


FIG. 1. (Color online) AFM images (300 nm×300 nm area) of typical QDs grown at different As BEP ($P$ series, left panel), crystallization temperatures ($T$ series, central panel), and initial droplet volumes ($V$ series, right panel). Sample numbers (see Table I) and QD heights are indicated alongside each image.

the As-terminated surface, a RHEED pattern corresponding to the Ga-stabilized (4×6) surface reconstruction was observed. The remaining volume of deposited Ga formed liquid Ga droplets. The crystallization, under As flux, of the Ga droplets into QDs was followed *in situ* by monitoring the appearance of transmission spots in the RHEED pattern.

Typical AFM images of a subset of the DE-QD are shown in Fig. 1. A large range of crystallization conditions and droplet volumes (from $10^2$ to $10^5$ $nm^3$) are explored. The DE-QDs approximatively have a truncated circular conical shape, and the DE-QD dimensions and aspect ratio exhibit a clear dependence on the growth conditions. The DE-QDs show a dependence of the lateral faceting on the initial Ga droplet volume [44] and the crystallization conditions. In particular, the DE-QDs belonging to the $P$ and $T$ series, although originating from identical Ga droplets, show a broad range of aspect ratios, with heights varying from 20 to 55 nm and DE-QD diameters ranging from 100 to 200 nm (see Fig. 2, in which typical AFM profiles of DE-QDs of the two series are reported).

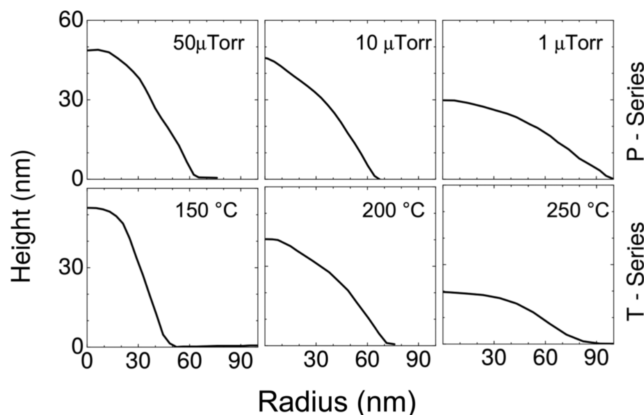


FIG. 2. AFM profiles of typical QDs grown at different As BEP ($P$ series) and crystallization temperatures ($T$ series)

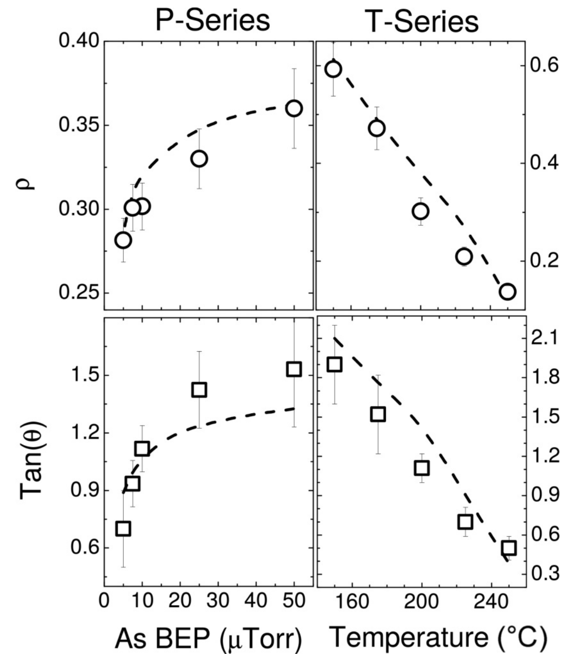


FIG. 3. Dependence, on the crystallization parameters, of the DE-QD aspect ration $\rho$ and facet angle $\theta$. $\theta$ is the angle between the QD facet and the substrate. Upper panels: $\rho$ dependence on As BEP (a) and crystallization temperature (b). Lower panels: $\theta$ dependence on As BEP (c) and crystallization temperature (d). The dashed lines indicate the theoretical prediction based on our model.

At high As flux and low crystallization temperature, the DE-QDs show a relatively high aspect ratio ($\rho = 0.6$). As the As flux decreases and/or the crystallization temperature increases, the DE-QD $\rho$ decreases (see Fig. 3) and the DE-QDs become slightly elongated along the $[1\bar{1}0]$ direction. None of the DE-QDs have straight facets. In the lower part of the DE-QDs, the exposed facets are steeper and well defined. In the upper part, the slope decreases, whereas the top is generally flat. We focused on the DE-QD aspect ratio and faceting. We defined the slope of facets as the tangent of the angle $\theta$ between the DE-QD surface and the substrate. Its dependence on the growth parameters is shown in Fig. 3. The facet orientation angle depends strongly on the As flux and on the crystallization temperature. The slope of the facet increases with increasing As flux and decreasing crystallization temperature.

X-STM makes it possible to analyze at the atomic scale the shape and the faceting of these DE-QDs after capping. This is of crucial importance as the capping layer has proven to affect strongly the final morphology of the QDs in the case of SK-QDs, where the capping layer can be engineered in order to introduce some degree of control in the SK-QDs height and shape [45]. Topographic images of a typical QD for different volumes of the initial Ga droplet are shown in Fig. 4. All the images were recorded at high negative bias voltages (−2.5 V). At these tunneling conditions and with the color scaling used, Al atoms give a darker electronic contrast than Ga atoms. Hence, the AlGaAs matrix (ternary compound) appears as an inhomogeneous region, while large, bright, homogeneous regions correspond to the GaAs nanostructures (binary compound). Four QD layers grown with different

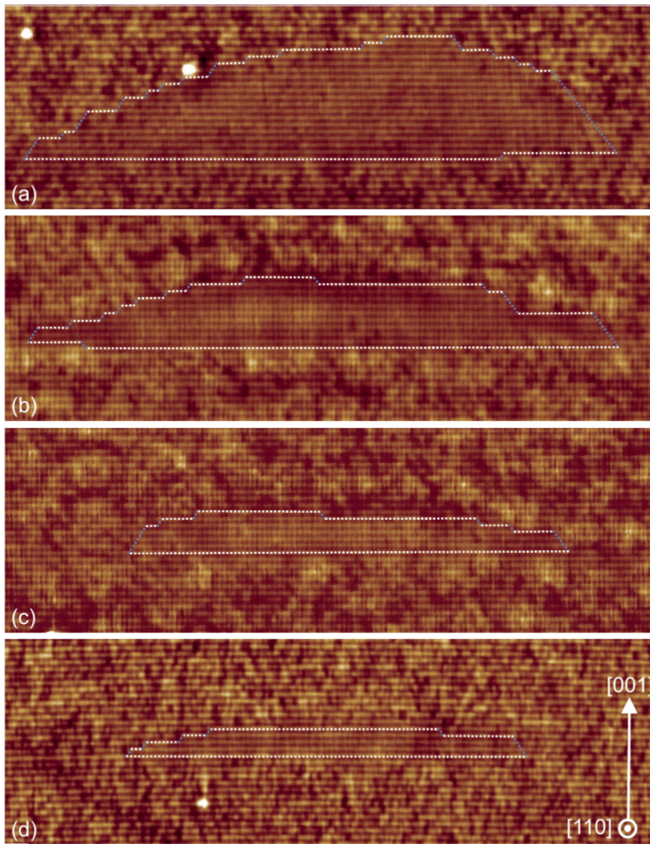


FIG. 4. (Color online) 53 nm×17 nm filled state topography images of QDs for (a) 5 ML, (b) 3 ML, (c) 2 ML. and (d) 1.5 ML of Ga. The images correspond to 2D cuts close to the center of the QDs. (110) facets are outlined in white and (111B) facets are outlined.

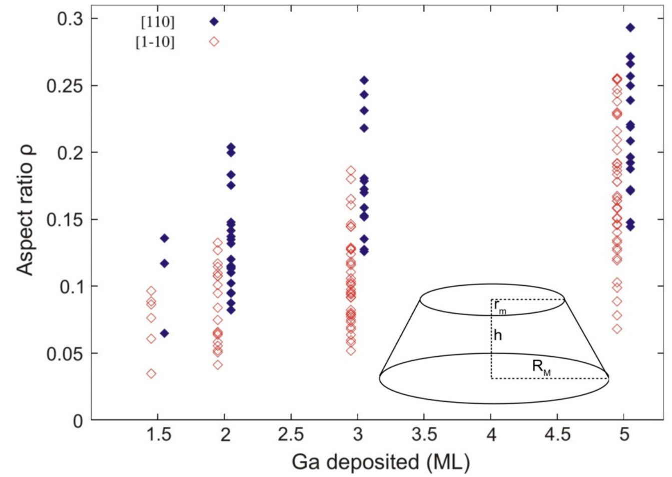


FIG. 5. (Color online) Aspect ratio as a function of the volume of Ga deposited for all the capped QDs analyzed by X-STM along the [110] direction (closed symbols) and $[1\bar{1}0]$ direction (open symbols). The aspect ratio does not depend linearly on the volume. The dispersion increases with the volume of Ga, indicating that (i) small QDs proportionally have a wider (001) top facet, (ii) the QD sides are not straight, and (iii) the angle $\theta$ is not constant. The difference between the [110] and the $[1\bar{1}0]$ directions reflects the elongation of the QDs along the $[1\bar{1}0]$ direction. Inset: schematic DE-QD shape.

volumes of Ga were studied, and 167 QDs were analyzed. Overall, the GaAs DE-QDs present fairly sharp interfaces and a low Al intermixing. $z$-profiles taken across the DE-QDs do not show any relaxation of the cleaved surface, implying that all these nanostructures are strain-free, as expected for lattice-matched AlGaAs/GaAs heterostructures. Also, independently from the volume of Ga used, the wetting layer is at most 2 ML thick, which is in agreement with Ga deposition on a $c(4\times4)$ reconstructed surface [23]. For this analysis, we make the assumption, supported by the AFM data, that the size distribution of the QDs is small. Thus if the QDs are approximatively of equal height, the height distribution for each layer observed by X-STM is due to the random position of the cleavage plane relative to the center of each QD. In this perspective, the highest QDs observed are considered as cut through their center. This way, we can attribute a standard QD height for 1.5, 2, 3, and 5 ML, respectively, of deposited Ga of 12 ML (3.4 nm), 16 ML (4.5 nm), 26 ML (7.3 nm), and 44 ML (12.4 nm). We found that the average QD diameter along the [110] direction increases with the volume of Ga from 35 nm for 1.5 ML Ga to 50 nm for 5 ML. An elongation of the diameters is observed in the $[1\bar{1}0]$ direction with respect to the [110] direction. This elongation originates from the anisotropic diffusion of Ga atoms during the annealing step [46]. The variation in height is much stronger than the variation in diameter with increasing volume of Ga. The change in aspect ratio along the [110] and $[1\bar{1}0]$ directions is illustrated in Fig. 5, where the QD aspect ratio is plotted against the volume of Ga deposited. In each direction, the aspect ratio does not depend linearly on the volume of Ga. Because of the arbitrary position of the cleavage, defining the exact shape of the QDs is difficult and has to be done carefully. From the X-STM images, we know that the QDs exhibit a (001) top facet. The absence of triangular-shaped cross sections and the fluctuations of cross-section base diameters within each layer exclude the possibility of truncated pyramidal QDs. This indicates a truncated shape with a circular base instead of a squared base, thus in agreement with AFM measurements. Moreover, as the volume of Ga increases, the aspect ratio dispersion in the cross-sectional STM cuts increases strongly, indicating that (i) small QDs proportionally have a wider (001) top facet, (ii) the QD sides are not straight, and (iii) the angle $\theta$ is not constant.

From AFM and X-STM images (Figs. 1, 2, and 4), the approximate DE-QD shape in the whole investigated growth parameter range is a truncated cone, whose major ($R_M$) and minor ($r_m$) radius and height ($h$) depend on the actual Ga droplet crystallization conditions (see the inset of Fig. 5). From experimental DE-QD profiles, we also find a proportionality between the major and minor radius of the DE-QDs: $r_m = \alpha R_M$, where $\alpha = 0.45$.

The data in the AFM series $P$, $T$, and $V$ show a continuous transition between surfaces with different orientation angles. This is a peculiar feature of the DE-QDs. To understand the surface structure of QDs that allows for such continuous tuning of surface facet orientation, AFM and X-STM accurate analyses of surfaces and interfaces have been carried out. Reference [47] reports that the DE-QDs sidewalls are characterized by stepped facets, which present a combination

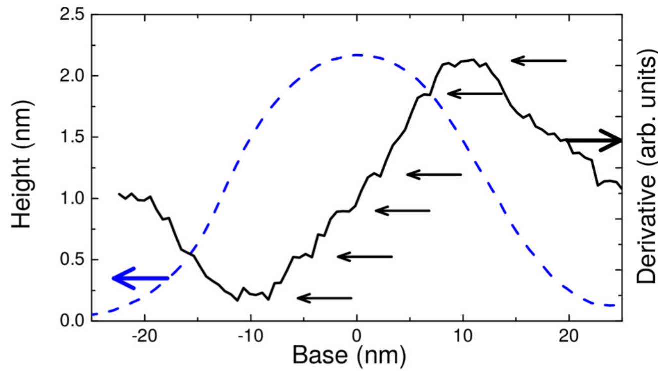


FIG. 6. (Color online) AFM profile (blue dashed line, left scale) and profile derivative (black line, right scale) of a QD belonging to sample $V3$. Black arrows indicate the appearance of plateaus on the profile derivative.

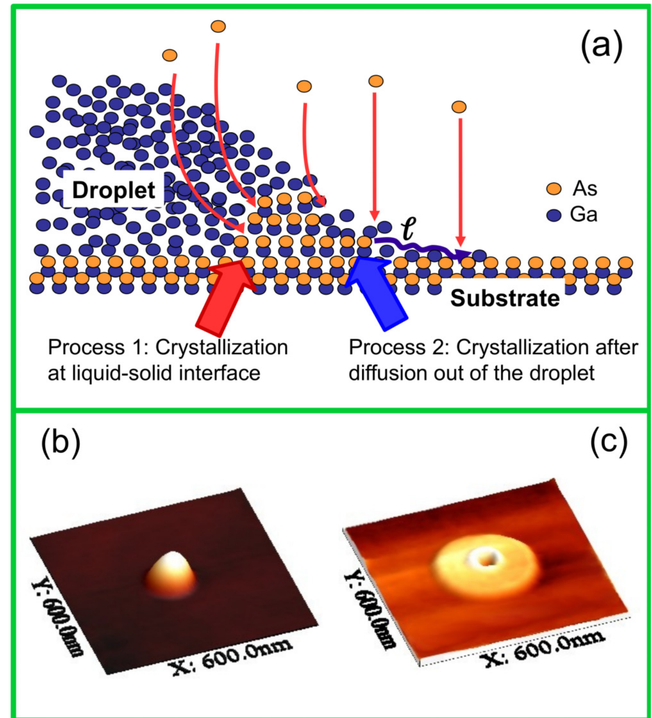


FIG. 7. (Color online) (a) Schematic explanation of the DE-QD growth mechanism during As supply. Process 1: As direct incorporation in the metallic droplet gives rise to GaAs crystallization at the liquid-solid interface, starting from the triple line. Process 2: Due to As adsorption on the surface surrounding the droplet, surface termination is changed and diffusion of Ga out of the droplet by capillary forces takes place. Coming from the droplets edge, Ga atoms can migrate covering a mean displacement length $\ell$ before being incorporated into the GaS crystal. Blue dots indicate Ga atoms. As atoms are indicated by yellow dots. (b) Typical AFM image of a DE-QD obtained As incorporation and Ga crystallization at the liquid-solid interface. (c) DE nanostructure fabricated by Ga diffusion controlled crystallization dynamics.

of alternating (001) terraces separated by (111)B facets. The presence of such stepped sidewalls can also be traced in our QDs. In Fig. 6 we report the AFM profile and its derivative of a DE-QD belonging to sample $V3$. Clear plateaus in the QD profile derivative are present, thus indicating a stepped morphology of the QD sidewalls.

The determination of facet orientation of the QD stepped sidewalls can be done in X-STM measurements, which allow for an atomic resolution of the interface morphology. As can be seen in Fig. 4, the DE-QD/barrier interfaces present the expected combination of alternating (001) terraces separated by (111)B facets [47]. The (001) facets are wider for DE-QDs with low $\rho$ and $\theta$ [Figs. 4(c) and 4(d)] than for those with a larger aspect ratio and facet angle [Figs. 4(a) and 4(b)]. As a result, the number of (111)B facets is much higher for the QDs with a high aspect ratio. Angles $\theta$ between 54° and 10° are obtained by an extension of (001) terraces and a reduction of (111)B steps when moving from high to low angle surfaces, allowing the system to expose minimal energy surfaces. Angles above 54°, observed at low $T$ and high As flux, may stem from the additional presence of {100} or {110} steps. The comparison and the good agreement between the AFM and X-STM data reveal the crucial point that the shape of the QDs is not altered upon capping. The dimensions and the exposed facets are preserved after capping.

## IV. DISCUSSION

The DE-QD aspect ratio and side facet angle appear to vary continuously in the range 0.05–0.6 and 10°–65°, respectively, by choosing the proper crystallization conditions. This is a peculiar characteristic of DE-QDs. In SK-QD systems, such as SiGe/Si and InAs/GaAs, well-defined transitions between aspect ratio and facet configurations are shown as a function of the deposited volume [48–50]. The three-dimensional island formation is in fact favored by the strain relaxation despite the higher surface energy. Surface energetics and strain relaxation play a fundamental role, and their ratio determines the overall dot shape [50].

The smooth variation in the DE-QD aspect ratio and side facet angle within wide ranges, depending only on the crystallization conditions, suggests a minor role played by surface energetics, compared to growth kinetics, in DE-QD formation. The DE-QD formation process is strongly influenced by the diffusion of Ga atoms out of the droplet toward thermodynamic equilibrium in the presence of an As flux [24,25,51], which is, for this system, a two-dimensional GaAs layer wetting the AlGaAs substrate.

The GaAs/AlGaAs DE-QD self-assembly thus strictly relies on the crucial and kinetically limited processes of crystallization and Ga diffusion [23]. During the Ga droplet crystallization under As flux, the relative importance of two processes proceeding in parallel determines the final crystal morphology (see Fig. 7) [23,52]:

(i) As incorporation in the metallic droplet and the GaAs crystallization at the liquid-solid interface.

(ii) As adsorption on the surface surrounding the droplet changing the surface termination and providing the thermodynamic driving force for the diffusion of Ga out of the droplet by capillary forces.

The As atoms impinging on the droplet during the crystallization step are dissolved into the liquid Ga. The GaAs crystallization then proceeds within the droplet by nucleation

at the triple point (see process 1 in Fig. 7) [53]. The crystalline GaAs formed at this stage is a ring at the perimeter of the droplet. The ring increases in thickness during As deposition and eventually merges to form a compact island [53]. At the same time, Ga adatom diffusion and Ga-As bond formation on the surface around the droplet lead to the accumulation of GaAs material within a diffusion length of Ga adatoms from the droplet edge (see process 2 in Fig. 7). Temperature and As pressure govern the relative weight of each process. The GaAs nanocrystal profile is therefore expected to be dependent on the ratio between the crystallization velocity at the liquid-solid interface within the droplet and the radial diffusion (and crystallization at the substrate surface) of Ga from the droplet edge. As a matter of fact, two extreme nanostructure morphologies are expected. In the case dominated by growth at the liquid-solid interface within the droplet, compact island morphologies are expected [Fig. 7(b)]; in the opposite case, when diffusion from the droplet edge controls the Ga crystallization dynamics, hollow morphologies, such as disks and rings, are expected [Fig. 7(b)] [23,52]. In between these two extremes, more complex morphologies, such as double rings and molecules, can be obtained [30,35,37,40].

In view of all these considerations, the main physical parameter governing the regimes for QD formation is the diffusion length of Ga from the droplet edge $\ell = \sqrt{4D_{\mathrm{Ga}}\tau}$, which depends on temperature and As flux through the diffusivity $D_{\mathrm{Ga}} = D_0 \exp(-E_A/kT)$ and the lifetime of the Ga adatoms $\tau$. Here $E_A$ is the activation energy of the diffusion process. The Ga adatom lifetime is $\tau = N_s/J_{\mathrm{As}}$, where $N_s$ is the number of surface sites and $J_{\mathrm{As}}$ is the atomic As flux [54,55]. This is the consequence of the As limited growth mode dominating in DE [23]. From our experimental data, we suggest that the accurate control of the Ga diffusion length, via temperature and As flux, allows us to finely tune the QD shape and dimensions.

To test our idea, we performed numerical simulations based on a diffusion model and compared them with the experimental DE-QD profiles. Our hypothesis is that the geometrical DE-QD profile is proportional to the local concentration profile of Ga diffusing from the droplet. Under this assumption, the Ga concentration profile before crystallization is $P(r) = A(r)/\xi$, where $A(r)$ is the experimental profile of the QD, in each series, crystallized at the lowest temperature or the highest As flux, and $\xi$ is the proportionality factor. This permits us to reduce the effects of the diffusion of Ga from the droplet perimeter (process 2) at minimum, and it allows us to implicitly take into account, at least to the first order of approximation, the complex crystallization dynamics inside the metallic Ga droplet (process 1) [52,53]. However, this makes the model outcome clearly dependent on the choice of $A(r)$. For this reason, we reduced the degree of arbitrariness by setting $A(r)$ to the more probable QD experimental profile within the ensembles in $T1$ (for the $T$ series) and $P1$ (for the $P$ series).

The QD radial profile, as a function of $\ell$, is then given by [56]

$$C(r,\ell) = \frac{2\xi}{\ell^2}\exp\left(\frac{-r^2}{\ell^2}\right)\int_0^\infty P(r') \times \exp\left(\frac{-r'^2}{\ell^2}\right) I_0\left(\frac{2rr'}{\ell^2}\right) r'dr'. \quad (1)$$

In our analysis, we disregard the anisotropy of the Ga diffusion [57]. In the definition of $\ell$, we set $D_0 = 0.7\ \mathrm{cm^2\,s^{-1}}$ and $E_A = 1.15$ eV, thus within the limits recently set for Ga adatom diffusion on As-terminated surfaces [55,58]. In Fig. 3 we report the comparison between $\rho$ and $\theta$ experimental results and the diffusion model for the $P$ and $T$ series. The description of the shape evolution given by the model is in excellent agreement with experimental data.

The actual DE-QD shape is then the outcome of a kinetically controlled (through the Ga diffusion length $\ell$) Ga diffusion and crystallization. Raising the substrate temperature, or decreasing As BEP, induces an increase of $\ell$ during the crystallization process. The change in aspect ratio and facet angle, which decrease with increasing $\ell$, can therefore be interpreted as a consequence of the increase of the DE-QD diameter due to diffusion of Ga out of the droplet.

On the basis of the demonstrated relevance of Ga diffusion in fixing the actual DE-QD shape, a quantitative and direct insight into the DE-QD morphology evolution with the growth parameters can be gained through a simple, parameter-free model, which describes the evolution of the DE-QD morphology as a function of droplet volume and crystallization condition.

As previously stated, the approximate DE-QD shape, in the whole investigated growth parameter range, is a truncated cone (see Fig. 5) with $r_m = \alpha R_M$, where $\alpha = 0.45$. The DE-QD volume $V$ is related to the initial droplet volume $V_0$ and radius $R_0$ via the relation $V = \beta V_0 = \beta\gamma R_0^3$. Assuming that each Ga atom in the droplet contributes to the formation of the DE-QD, because of the low crystallization temperature, $\beta$ is the ratio $\beta = V_{\mathrm{GaAs}}/V_{\mathrm{Ga}} = 2.31$ between the volume $V_{\mathrm{GaAs}} = 4.52\times10^{-29}\ \mathrm{m^3}$ of a GaAs molecule inside the GaAs crystal and the atomistic volume of Ga in the liquid droplet, $V_{\mathrm{Ga}} = 1.96\times10^{-29}\ \mathrm{m^3}$. The proportionality constant $\gamma$ is set by the contact angle between the metallic Ga and the substrate. $\gamma = 0.7$ in our experiments.

Under As pressure, the Ga diffusion on the As-terminated surface increases the radius of the DE-QD base by a diffusion length: $R_M = R_0 + \ell$. Changing the diffusion length $\ell$ via temperature and As flux, at constant QD volume $V$, directly affects the QD height and facet through the dependence of $R_M$ on $\ell$. Increasing the DE-QD radius at constant DE-QD volume therefore reduces the DE-QD height and consequently the DE-QD aspect ratio $\rho = h/2R_M$ and the facet angle $\tan(\theta) = h/(R_M - r_m)$. With simple geometrical considerations, we can express $\theta$ and $\rho$ as a function of the ratio of two observable quantities, namely the droplet ($R_0$) and the DE-QD ($R_M$) radius:

$$\tan(\theta) = \frac{3}{\pi}\frac{\beta\gamma}{(1-\alpha^3)}\left(\frac{R_0}{R_M}\right)^3, \quad (2)$$

$$\rho = \frac{3}{2\pi}\frac{\beta\gamma}{(1+\alpha+\alpha^2)}\left(\frac{R_0}{R_M}\right)^3. \quad (3)$$

Equations (2) and (3) are fit parameter-free and independent of the actual growth conditions. The agreement between the predicted behavior and the experimental data of both $\theta$ and $\rho$, shown in Fig. 8, is remarkable, thus indicating once again the fundamental role played by Ga diffusion during As-induced crystallization in determining the final DE-QD morphology.

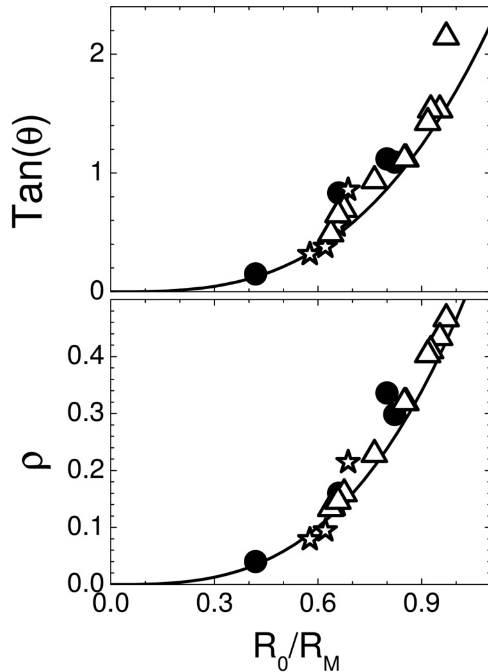


FIG. 8. Left panel: facet angle $\theta$, and right panel: aspect ratio $\rho$ as a function of the $R_0/R_M$ ratio for the sets $P$ and $T$ (triangles), $V$ (circles), and the series $V_{cap}$ (stars). The continuous lines are the theoretical prediction obtained using Eqs. (2) and (3).

It is worth noting that Eqs. (2) and (3) predict the dependence of $\rho$ and $\theta$ on the initial droplet volume at fixed crystallization conditions, which was observed in sample series $V$ and $V_{cap}$ and Ref. [44]. Fixing substrate temperature and As BEP during crystallization sets the Ga diffusion length $\ell$ in the experiments. This makes $R_0/R_M = (1+\ell/R_0)^{-1}$ an increasing function of the droplet volume $V_0$. Therefore, our theory predicts that the DE-QD aspect ratio and the facet orientation angle will increase with the droplet volume. As a matter of fact, changing the initial droplet volume has only a minor effect on $R_M$ as $R_0 \propto V_0^{1/3}$, so the increase of the final DE-QD volume affects QD height only. Again, no sharp transition on the dependence of $\rho$ and $\theta$ on $R_0/R_M$ is observed, as expected for a system driven by energy minimization and not influenced by any minima in the QD morphology energy landscape.

A fundamental outcome of Eqs. (2) and (3), together with the possibility, given by DE, to determine the QD volume by the initial Ga droplet, is that DE-QD size and aspect ratio can be independently engineered by a suitable choice of the Ga deposition and As crystallization conditions. This is of the utmost importance when a fine tuning of the QD electronic properties is necessary to improve QD-based devices, such as single-photon emitters, detectors, or solar cells [10,13,16]. Simple electronic quantum confinement considerations, in fact, indicate that the ability to control independently QD size and aspect ratio permits the independent control of QD emission energy and electronic interlevel energy spacing. The latter is extremely relevant in shaping electron-phonon interaction in QDs [59–62], a fundamental property of QDs for the improvement of quantum devices at room temperature [63,64].

A post-droplet-crystallization annealing procedure performed on sample $V_{cap}$ induces a slight change in the QD morphology related to thermally activated mass transport processes driven by the out-of-equilibrium state of DE-QDs [46,65]. Overall, however, the QD morphology is maintained upon capping. Our growth model is still valid after capping and rapid thermal annealing. Also the X-STM data ($V_{cap}$ series) align along the Eqs. (2) and (3) lines in Fig. 8.

## V. CONCLUSIONS

DE-QD morphology is completely determined by the kinetics of droplet Ga crystallization under As flux. The two relevant quantities that set the actual DE-QD shape are the initial droplet volume and the Ga diffusion length $\ell$ at the droplet crystallization conditions. This permits us to independently control the size and aspect ratio of GaAs/AlGaAs DE-QDs over wide ranges. The QD faceting undergoes a continuous transition that depends on the initial droplet radius and the diffusion length at the crystallization conditions only. The facets are made up of a series of steps consisting of 001 and 111 facets whose length varies depending on the facet angle. The QD morphology is maintained upon capping. Parameter-free simple analytical relations are introduced [Eqs. (2) and (3)], which make it possible to create a detailed engineering of the QD electronic properties via growth condition control. Although it is based on the simple mechanism of controlled diffusion during crystallization, the DE-QD shape engineering mechanism is extremely powerful. It permits the independent achievement of usually incompatible targets, namely QD emission; interband, intervalley, spin-orbit, and strain-induced state coupling [4,5]; and electron-phonon scattering [62].

## ACKNOWLEDGMENT

The research was supported in Italy by Fondazione Cariplo (Project COSMOS - 2013-1775). The authors thank D. Scarpellini for help.

[1] M. A. Kastner, Phys. Today 46(1), 24 (1993).
[2] D. Bimberg, M. Grundmann, and N. N. Ledentsov, *Quantum Dots Heterostructures* (Wiley, New York, 1999).
[3] C. Delerue and M. Lannoo, *Nanostructures-Theory and Modeling* (Springer-Verlag, Berlin, 2004).
[4] G. A. Narvaez, G. Bester, and A. Zunger, Phys. Rev. B **72**, 245318 (2005).
[5] J.-W. Luo and A. Zunger, Phys. Rev. B **84**, 235317 (2011).
[6] E. A. Zibik, T. Grange, B. A. Carpenter, N. E. Porter, R. Ferreira, G. Bastard, D. Stehr, S. Winnerl, M. Helm, H. Y. Liu, M. S. Skolnick, and L. R. Wilson, Nat. Mater. **8**, 803 (2009).
[7] A. Tredicucci, Nat. Mater. **8**, 775 (2009).
[8] G. M. Vanacore, J. Hu, W. Liang, S. Bietti, S. Sanguinetti, and A. H. Zewail, Nano Lett. **14**, 6148 (2014).
[9] P. Bhattacharya and Z. Mi, Proc. IEEE **95**, 1723 (2007).
[10] P. Martyniuk and A. Rogalski, Prog. Quantum Electron. **32**, 89 (2008).
[11] G. Scalari, C. Walther, M. Fischer, R. Terazzi, H. Beere, D. Ritchie, and J. Faist, Laser Photon. Rev. **3**, 45 (2009).

[12] T. Akiyama, M. Ekawa, M. Sugawara, K. Kawaguchi, A. Kuramata, H. Ebe, and Y. Arakawa, IEEE Photon. Technol. Lett. **17**, 1614 (2005).
[13] S. Strauf, N. G. Stoltz, M. T. Rakher, L. A. Coldren, P. M. Petroff, and D. Bouwmeester, Nat. Photon. **1**, 704 (2007).
[14] L. Cavigli, S. Bietti, N. Accanto, S. Minari, M. Abbarchi, G. Isella, C. Frigeri, A. Vinattieri, M. Gurioli, and S. Sanguinetti, Appl. Phys. Lett. **100**, 231112 (2012).
[15] A. Luque and A. Marti, Phys. Rev. Lett. **78**, 5014 (1997).
[16] A. Mellor, A. Luque, I. Tobias, and A. Marti, Appl. Phys. Lett. **101**, 133909 (2012).
[17] A. Scaccabarozzi, S. Adorno, S. Bietti, M. Acciarri, and S. Sanguinetti, Phys. Status Solidi–Rapid Res. Lett. **7**, 173 (2013).
[18] A. D. Yoffe, Adv. Phys. **51**, 799 (2002).
[19] X. Li, Y. Wu, D. Steel, D. Gammon, T. H. Stievater, D. S. Katzer, D. Park, C. Piermarocchi, and L. J. Sham, Science **301**, 809 (2003).
[20] C. L. Salter, R. M. Stevenson, I. Farrer, C. A. Nicoll, D. A. Ritchie, and A. J. Shields, Nature (London) **465**, 594 (2010).
[21] S. Kiravittaya, A. Rastelli, and O. G. Schmidt, Rep. Prog. Phys. **72**, 046502 (2009).
[22] J. T. Robinson, A. Rastelli, O. Schmidt, and O. D. Dubon, Nanotechnology **20**, 085708 (2009).
[23] S. Sanguinetti and N. Koguchi, in *Molecular Beam Epitaxy—From Research to Mass Production*, edited by M. Henini (Elsevier, Amsterdam, 2013), Chap. 4, p. 95.
[24] N. Koguchi and K. Ishige, J. Vac. Sci. Technol. B **11**, 787 (1993).
[25] K. Watanabe, N. Koguchi, and Y. Gotoh, Jpn. J. Appl. Phys. **39**, L79 (2000).
[26] T. Kuroda, S. Sanguinetti, M. Gurioli, K. Watanabe, F. Minami, and N. Koguchi, Phys. Rev. B **66**, 121302(R) (2002).
[27] J. G. Keizer, J. Bocquel, P. M. Koenraad, T. Mano, T. Noda, and K. Sakoda, Appl. Phys. Lett. **96**, 062101 (2010).
[28] B. Liang, A. Lin, N. Pavarelli, C. Reyner, J. Tatebayashi, K. Nunna, J. He, T. J. Ochalski, G. Huyet, and D. L. Huffaker, Nanotechnology **20**, 455604 (2009).
[29] A. Urbanczyk, J. G. Keizer, P. M. Koenraad, and R. Notzel, Appl. Phys. Lett. **102**, 073103 (2013).
[30] T. Mano, T. Kuroda, S. Sanguinetti, T. Ochiai, T. Tateno, J. S. Kim, T. Noda, M. Kawabe, K. Sakoda, G. Kido, and N. Koguchi, Nano Lett. **5**, 425 (2005).
[31] Z. M. Wang, K. Holmes, J. L. Shultz, and G. J. Salamo, Phys. Status Solidi **202**, R85 (2005).
[32] M. Jo, J. G. Keizer, T. Mano, P. M. Koenraad, and K. Sakoda, Appl. Phys. Express **4**, 055501 (2011).
[33] J. G. Keizer, M. Jo, T. Mano, T. Noda, K. Sakoda, and P. M. Koenraad, Appl. Phys. Lett. **98**, 193112 (2011).
[34] M. Hanke, M. Schmidbauer, D. Grigoriev, P. Schafer, R. Kohler, T. H. Metzger, Z. M. Wang, Y. I. Mazur, and G. J. Salamo, Appl. Phys. Lett. **89**, 053116 (2006).
[35] M. Yamagiwa, T. Mano, T. Kuroda, T. Tateno, K. Sakoda, G. Kido, N. Koguchi, and F. Minami, Appl. Phys. Lett. **89**, 113115 (2006).
[36] M. DeJarld, K. Reyes, P. Smereka, and J. M. Millunchick, Appl. Phys. Lett. **102**, 133107 (2013).
[37] C. Somaschini, S. Bietti, N. Koguchi, and S. Sanguinetti, Nano Lett. **9**, 3419 (2009).
[38] C. Somaschini, S. Bietti, N. Koguchi, and S. Sanguinetti, Nanotechnology **22**, 185602 (2011).
[39] C. Somaschini, S. Bietti, S. Sanguinetti, N. Koguchi, and A. Fedorov, Nanotechnology **21**, 125601 (2010).
[40] C. Somaschini, S. Bietti, N. Koguchi, and S. Sanguinetti, Appl. Phys. Lett. **97**, 203109 (2010).
[41] T. Mano, M. Abbarchi, T. Kuroda, C. A. Mastrandrea, A. Vinattieri, S. Sanguinetti, K. Sakoda, and M. Gurioli, Nanotechnology **20**, 395601 (2009).
[42] S. Sanguinetti, K. Watanabe, T. Tateno, M. Gurioli, P. Werner, M. Wakaki, and N. Koguchi, J. Cryst. Growth **253**, 71 (2003).
[43] A. Ohtake, Surf. Sci. Rep. **63**, 295 (2008).
[44] C. Heyn, A. Stemmann, A. Schramm, H. Welsch, W. Hansen, and A. Nemcsics, Appl. Phys. Lett. **90**, 203105 (2007).
[45] J. G. Keizer, M. Bozkurt, J. Bocquel, T. Mano, T. Noda, K. Sakoda, E. C. Clark, M. Bichler, G. Abstreiter, J. J. Finley, W. Lu, T. Rohel, H. Folliot, N. Bertru, and P. M. Koenraad, J. Appl. Phys. **109**, 102413 (2011).
[46] S. Adorno, S. Bietti, and S. Sanguinetti, J. Cryst. Growth **378**, 515 (2013).
[47] A. Nemcsics, L. Tóth, L. Dobos, and A. Stemmann, Microelectron. Reliab. **51**, 927 (2011).
[48] A. Rastelli and H. von Känel, Surf. Sci. **532–535**, 769 (2003).
[49] A. Rastelli, M. Stoffel, J. Tersoff, G. S. Kar, and O. G. Schmidt, Phys. Rev. Lett. **95**, 026103 (2005).
[50] G. Costantini, A. Rastelli, C. Manzano, P. Acosta-Diaz, G. Katsaros, R. Songmuang, O. Schmidt, H. V. Känel, and K. Kern, J. Cryst. Growth **278**, 38 (2005).
[51] C. D. Lee, C. Park, H. J. Lee, S. K. Noh, K. S. Lee, and S. J. Park, Appl. Phys. Lett. **73**, 2615 (1998).
[52] K. Reyes, P. Smereka, D. Nothern, J. M. Millunchick, S. Bietti, C. Somaschini, S. Sanguinetti, and C. Frigeri, Phys. Rev. B **87**, 165406 (2013).
[53] S. Bietti, C. Somaschini, and S. Sanguinetti, Nanotechnology **24**, 205603 (2013).
[54] H. Neave, P. J. Dobson, B. A. Joyce, and J. Zhang, Appl. Phys. Lett. **47**, 100 (1985).
[55] S. Bietti, C. Somaschini, L. Esposito, A. Fedorov, and S. Sanguinetti, J. Appl. Phys. **116**, 114311 (2014).
[56] J. Crank, *The Mathematics of Diffusion* (Clarendon Press, Oxford, 1955).
[57] K. Ohta, T. Kojima, and T. Nakagawa, J. Cryst. Growth **95**, 71 (1989).
[58] V. P. Labella, D. W. Bullock, Z. Ding, C. Emery, W. G. Harter, and P. M. Thibado, J. Vac. Sci. Technol. A **18**, 1526 (2000).
[59] P. Gartner, J. Seebeck, and F. Jahnke, Phys. Rev. B **73**, 115307 (2006).
[60] S. Sanguinetti, M. Guzzi, E. Grilli, M. Gurioli, L. Seravalli, P. Frigeri, S. Franchi, M. Capizzi, S. Mazzuccato, and A. Polimeni, Phys. Rev. B **78**, 085313 (2008).
[61] K. Schuh, P. Gartner, and F. Jahnke, Phys. Rev. B **87**, 035301 (2013).
[62] A. Steinhoff, H. Kurtze, P. Gartner, M. Florian, D. Reuter, A. D. Wieck, M. Bayer, and F. Jahnke, Phys. Rev. B **88**, 205309 (2013).
[63] M. R. Dachner, E. Malic, M. Richter, A. Carmele, J. Kabuss, A. Wilms, J. E. Kim, G. Hartmann, J. Wolters, U. Bandelow, and A. Knorr, Phys. Status Solidi Basic Res. **247**, 809 (2010).
[64] P. Kaer, N. Gregersen, and J. Mork, New J. Phys. **15**, 035027 (2013).
[65] M. Jo, T. Mano, and K. Sakoda, Appl. Phys. Express **3**, 045502 (2010).